Published OnlineFirst April 20, 2010; DOI: 10.1158/1541-7786.MCR-09-0497

Molecular Cancer Research

Targeted Knockdown of SEPT9_v1 Inhibits Tumor Growth and Angiogenesis of Human Prostate Cancer Cells Concomitant with Disruption of Hypoxia-Inducible Factor-1 Pathway

Sharon Amir, Maya Golan, and Nicola J. Mabjeesh

Abstract

Hypoxia-inducible factor-1 (HIF-1) is a key transcription factor in the hypoxic response pathway. We recently identified a novel interaction between HIF-1α and the mammalian septin family member, septin 9 protein, isoform 1 (SEPT9_i1), a protein product of septin 9 transcript variant 1 (SEPT9_v1). Septins are a highly conserved family of GTP-binding cytoskeletal proteins that are implicated in multiple cellular functions, including oncogenesis. SEPT9_i1 binds and stabilizes HIF-1α protein and stimulates HIF-1 transcriptional activity by preventing its RACK1-mediated ubiquitination and degradation. SEPT9_i1–HIF-1 activation promotes tumor growth and angiogenesis. The effect of SEPT9_v1 silencing in prostate cancer cells was studied. SEPT9_v1 stable knockdown was generated in PC-3 cells using a specific shRNA. SEPT9_v1 silencing reduced HIF-1α protein expression and inhibited HIF-1 transcriptional activity. SEPT9_v1 knockdown affected cell morphology, deregulated cell cycle, and decreased migration. The antiproliferative effect of shSEPT9_v1 was abolished in HIF-1α knockout colon cancer cells. *In vivo*, SEPT9_i1 depletion reduced HIF-1α protein expression, cellular proliferation, tumor growth, and angiogenesis. These results provide new insights and validation for applying SEPT9_v1 as a potential target for antitumor therapy by interrupting the HIF-1 pathway. *Mol Cancer Res; 8(5); 643–52. ©2010 AACR.*

Introduction

Hypoxia exists in solid tumors and is often associated with resistance to radiation therapy and chemotherapy, selection of more invasive and metastatic clones, and poorer prognosis (1-3). Hypoxia-inducible factor-1 (HIF-1) is a key transcription factor for cells to respond and adapt to survive hypoxia (4). HIF-1 target genes encode proteins involved in anaerobic metabolism (e.g., glycolytic enzymes and glucose transporters), angiogenesis [e.g., vascular endothelial growth factor (VEGF)], and erythropoiesis (e.g., erythropoietin; ref. 4). HIF-1 is a heterodimer consisting of a constitutively expressed subunit, HIF-1β, and an oxygen-regulated subunit, HIF-1α. HIF-1 transcriptional activity is directly affected by the abundance and stability of HIF-1α.

Authors' Affiliation: Prostate Cancer Research Laboratory, Department of Urology, Tel Aviv Sourasky Medical Center, Sackler Faculty of Medicine, Tel Aviv University, Tel Aviv, Israel

Note: Supplementary data for this article are available at Molecular Cancer Research Online (http://mcr.aacrjournals.org/).

This work was done in partial fulfillment of the requirements for a Ph.D. degree of S. Amir.

Corresponding Author: Nicola J. Mabjeesh, Department of Urology, Tel Aviv Sourasky Medical Center, 6 Weizman Street, Tel Aviv 64239, Israel. Phone: 972-3-6974544; Fax: 972-3-6973183. E-mail: nicolam@tasmc.health.gov.il

doi: 10.1158/1541-7786.MCR-09-0497

In tumor cells, HIF-1 can also be regulated and activated by other genetic factors, such as oncogenes (Ras and phosphoinositide 3-kinase) or loss of tumor suppressors (VHL or PTEN) even under aerobic conditions (1). Overexpression of HIF-1α has been shown in many human cancers and is associated with poor prognosis and treatment failure (1). Therefore, HIF-1 inhibition has become an attractive therapeutic strategy to target cancer cells (5-7).

We recently described another novel activation pathway of HIF-1 under normoxia by a member of the mammalian septin family, septin 9 protein, isoform 1 (SEPT9_i1), a product of septin 9 transcript variant 1 (SEPT9_v1; ref. 8). Mammalian septins are evolutionary conserved proteins that form filaments associated with cytoskeleton organization, membrane dynamics, mitosis, cytokinesis, and cell cycle progression (9, 10). Recently, accumulating data suggest that some septin family members also participate in the pathogenesis of neoplasia (11) and neurodegenerative diseases (12). We had shown that SEPT9_i1 interacts with HIF-1α, but not with HIF-2α, to prevent its RACK1-mediated ubiquitination and degradation (13) and that SEPT9_i1 protein activates HIF-1 transcriptional activity and increases tumor growth and angiogenesis in prostate cancer xenografts (8). Similarly, Gonzalez et al. (14) showed that high expression of SEPT9_i1 is also associated with accelerated growth kinetics and increased motility in human breast cancer cells. Another line of evidence supporting the role of *SEPT9* in oncogenesis is derived from

Published OnlineFirst April 20, 2010; DOI: 10.1158/1541-7786.MCR-09-0497

prostate cancer tumors with the chromosomal fusion between the transmembrane protease Ser^2 (TMPRSS2) and ERG, a member of the erythroblast transformation-specific transcription factor family (15). These tumors express significantly higher *SEPT9* levels compared with tumors without the translocation and are associated with a more aggressive clinical course (16).

In the current study, we tested the hypothesis that disruption of the SEPT9_i1–HIF-1α pathway by applying RNAi methodology would be affective in inhibiting angiogenesis and tumor growth in prostate cancer. We provide evidence that SEPT9_v1 could serve as a new target for therapy in prostate cancer.

Materials and Methods

Cell culture and hypoxia treatment. Human prostate cancer PC-3 cells were maintained in RPMI 1640; Colo-357, MIA, and Panc1 cells were maintained in DMEM; and HCT116 cells were maintained in modified McCoy's medium. Parental HCT116 ($HCT116^{P}$) and $HCT116^{HIF\text{-}1\alpha-/-}$ were designed by Dang et al. (17) and kindly obtained as a generous gift from Dr. Long Dang (University of Florida, Gainesville, FL). These cells were maintained in McCoy's 5A medium and passed in parallel to preserve the same passage number. All of the media were supplemented with 10% FCS and antibiotics. The cells were cultured at 37°C in a humidified atmosphere and 5% CO_2 in air. For hypoxic exposure, the cells were placed in a sealed modular incubator chamber (Billups-Rothenberg) flushed with 1% O_2, 5% CO_2, and 94% N_2 and then cultured at 37°C for 16 hours.

Antibodies. The following primary antibodies were used: rabbit polyclonal antibody to SEPT9_i1 [previously produced and characterized (8)], rabbit polyclonal against general SEPT9 (recognizes all isoforms; Abgent), mouse monoclonal anti–HIF-1α (BD Biosciences), mouse monoclonal anti-hemagglutinin (HA; Covance), mouse monoclonal anti–α-tubulin (Sigma-Aldrich), goat polyclonal anti–TOPO-I and anti–β-actin (Santa Cruz Biotechnology, Inc.), mouse monoclonal anti-CD34 and anti-Ki67 (Dako-Cytomation), and rabbit polyclonal activated caspase-3 (Cell Signaling). Secondary antibodies used for Western blotting were horseradish peroxidase conjugated (Jackson ImmunoResearch) and those used for immunohistochemistry were MACH 3 Rabbit HRP Polymer (Biocare Medical).

shRNA viral vector construction. Oligonucleotides corresponding to sequences taken from the unique NH_2 terminus of SEPT9_v1 were designed (5′-GATCCCCGAAGTCTTACTCAGGAGGCttcaagagaGCCTCCTGAGTAAGACTTCTTTTTA-3′ and 5′-AGCTTAAAAAGAAGTCTTACTCAGGAGGCtctcttgaaGCCTCCTGAGTAAGACTTCGGG-3′) and constructed into pSUPER.retro.puro (OligoEngine) as previously described (18).

Retroviral infection and stable expression of shSEPT9_v1 in PC-3 cells. Stable expression of shSEPT9_v1 in PC-3 cells was established previously in our lab (18). Briefly, PC-3 cells were infected by supernatants containing retroviral particles of pSUPER.retro empty vector (EV) and pSUPER.retro expressing shRNA to green fluorescent protein (GFP) or to SEPT9_v1. Cells were selected for puromycin (5 mg/mL) resistance and screened for SEPT9_i1 downregulation.

Protein extraction and Western blot. Whole-cell extract (WCE) and nuclear extract were prepared and analyzed as previously described (19). Protein concentration was determined using a bicinchoninic acid protein assay kit (Pierce). Protein extracts were analyzed by SDS-PAGE and immunoblotted with the displayed antibodies in the figures.

Hypoxia response element–dependent luciferase assay. Hypoxia response element (HRE)–dependent luciferase activity was determined using the pBI-GL construct (pBI-GL V6L) containing six tandem copies of the *VEGF* HRE as previously described (20, 21). Briefly, cells were seeded in six-well plates and transfected with a total of 1 μg of reporter plasmid per well using GenePorter transfection reagent (Gene Therapy Systems, Inc.). Duplicate sets of transfected cell culture dishes were then separated and incubated under normoxic and hypoxic conditions for 16 hours. Luciferase enzymatic activity was measured with a commercial kit (Tropix) using a BMG Labtechnologies LUMIstar Galaxy luminometer following the manufacturer's instructions. Arbitrary luciferase activity units were normalized to the amount of protein in each assay point.

Ubiquitination assay. Cells were seeded in 100-mm plates and transiently transfected with 5 μg pEF1a plasmid expressing HA-ubiquitin (a generous gift from Prof. Y. Yarden, Weizmann Institute of Science, Rehovot, Israel) as described above. After 48 hours, the cells were lysed in 20 mmol/L HEPES (pH 7.5), 0.1 mol/L NaCl, 2 mmol/L EDTA, 0.5% NP40, and 10% glycerol. Protease and phosphatase inhibitors were added to the lysis buffer. The lysates were centrifuged at 14,000 rpm for 15 minutes at 4°C. Ten percent of the WCE was kept for input analysis, and the rest was incubated with HIF-1α antibody overnight at 4°C. The lysates were then rotated with protein G–Sepharose (Sigma-Aldrich) for 2 hours at 4°C. The beads were washed and eluted in 2× Laemmli sample buffer, analyzed by SDS-PAGE, and immunoblotted with HIF-1α and HA antibodies.

RNA isolation and quantitative real-time reverse transcription-PCR. Total RNA was extracted from cells using NucleoSpin RNA II kit (Macherey-Nagel) following the manufacturer's instructions. One microgram of total RNA was reverse transcribed into cDNA using Verso cDNA kit (Abgene) using anchored oligo(dT) as first-strand primer. Quantitative real-time PCRs were done with primers specific to SEPT9_v1 (forward: GAAGAAGTCTTACTCAGGAGGC; reverse: CTCCTCGACCTCAAAAGATC), *VEGF*, endothelin-1 (*ET-1*), glucose transporter-1 (*Glut-1*), and *β-actin* genes in duplicates using LightCycler FastStart DNA Master SYBR Green I (Roche Applied Science) as described (8). The PCRs were done at a total volume of 10 μL using

Published OnlineFirst April 20, 2010; DOI: 10.1158/1541-7786.MCR-09-0497

3 mmol/L $MgCl_2$ and 0.5 μmol/L of each primer. The expression of the each gene was normalized using β-actin expression levels.

Cell cycle analysis (fluorescence-activated cell sorting). Cells were collected in ice-cold PBS (50,000 cells/mL) and stained with 50 μL propidium iodide (1 mg/mL) and 50 μL of 1% Triton. Cell cycle distribution was detected by flow cytometry (FACSort, Becton Dickinson) using CellQuest software.

Cytospin. Cells (5,000) were suspended in 100 μL PBS and in a cytocentrifuge cup, which was preplaced in a Shandon cytocentrifuge 4 (Thermo Electron). After centrifugation at 700 rpm for 5 minutes at room temperature and drying in air, the cytospin slides were stained with Giemsa (Sigma-Aldrich) and analyzed by light microscopy.

Scratch wound assay. Cells were grown to confluence in six-well plates. After 24 hours, the monolayers were scratched using a 200 μL sterile plastic pipette tip and washed twice with complete medium. The cells were allowed to migrate onto a plastic surface and photographed. Wound-healing inhibition was quantified by using ImageJ software available from the NIH Web site as described (22). Two random pictures were taken for each wound immediately after the wound was inflicted to the cell monolayer and after 4, 8, and 24 hours. The pictures were uploaded into the ImageJ software, the area of the wound was measured by using the rectangle area selection tool, and the two areas per well were averaged. The percentage of wound healed was then calculated using the following formula: 100 − (final area/initial area × 100%).

2,3-Bis[2-methoxy-4-nitro-5-sulfophenyl]-2H-tetrazolium-5-carboxanilide inner salt proliferation assay. Cells (2,000-5,000 per well) were seeded in 96-well plates in a volume of 200 μL for cell proliferation assay using a 2,3-bis[2-methoxy-4-nitro-5-sulfophenyl]-2H-tetrazolium-5-carboxanilide inner salt (XTT) kit (Biological Industries Ltd.). XTT reagent was added in triplicates for each time point and processed as previously described (8).

Tumor model. Different clones of EV control and shSEPT9_v1 PC-3 cells (2×10^6) were injected s.c. into the back of athymic nude mice. All procedures were done in compliance with the Tel Aviv Sourasky Medical Center Animal Care and Use Committee and NIH guidelines. The animals were monitored for tumor development twice a week. Tumor dimensions were measured with calipers, and tumor volume was calculated according to the following formula: tumor volume = $\text{width}^2 \times \text{length}/2$. The animals were sacrificed before the tumors reached >1,000 mm^3 or when the mice started to lose weight. The tumors were excised and cut into two pieces. One piece of tumor was fixed with 4% buffered formalin for immunohistochemical staining, and the rest of the tumor was immediately frozen in liquid N_2 and kept at −80°C for protein extraction.

Immunohistochemical staining. Paraffin-embedded tissue was sectioned into 3-μm thickness, mounted on SuperFrost/Plus slides (Menzel-Gläser), and immunostained as described elsewhere (23). Sections were dewaxed and hydrated through graded ethanols, cooked in a pressure cooker at 115°C for 3 minutes (decloaking chamber, Biocare Medical) for antigen retrieval in a suitable calibrated buffer

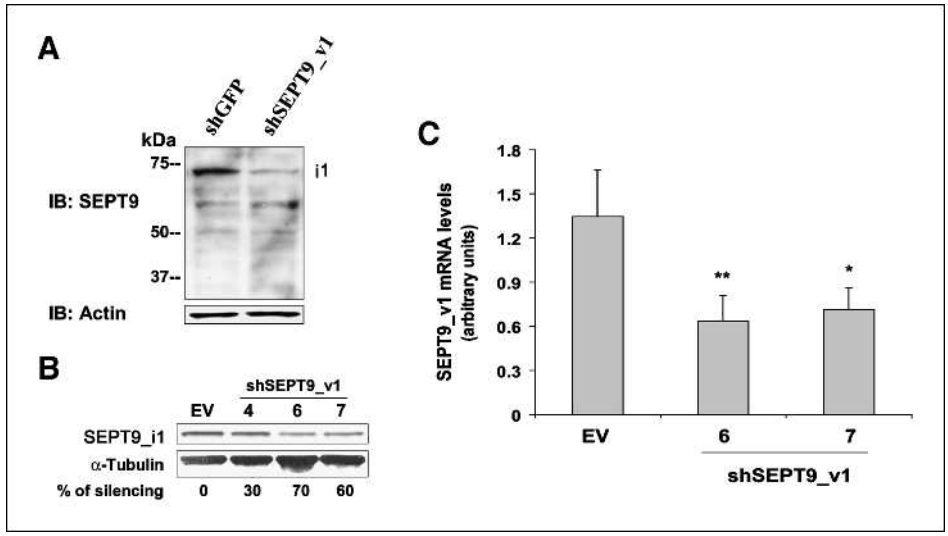

FIGURE 1. Specific SEPT9_v1 silencing in prostate cancer cells. A, PC-3 cells were infected by retroviral vectors (pSUPER.retro.puro) carrying either shRNA to GFP or shRNA to SEPT9_v1. WCEs were prepared, analyzed by SDS-PAGE, and immunoblotted with antibodies directed against a conserved region within the COOH terminus of SEPT9 (recognizes all isoforms) and then reprobed with antibodies to actin. B, infected PC-3 cells with the EV control or with shSEPT9_v1 were grown in the presence of puromycin. Extracts from puromycin-resistant clones were analyzed for SEPT9_i1 downregulation by SDS-PAGE and immunoblotting with specific antibodies to SEPT9_i1 (recognizes only SEPT9_i1) and to α-tubulin. C, total RNA was isolated from puromycin-resistant EV cells and shSEPT9_v1 clones 6 and 7 were grown under normoxia. Real-time PCR was done to amplify SEPT9_v1 and β-actin mRNA. Normalized mRNA levels to β-actin were drawn. Columns, mean (n = 4); bars, SD. *, P = 0.01; **, P = 0.007, compared with EV.

Published OnlineFirst April 20, 2010; DOI: 10.1158/1541-7786.MCR-09-0497

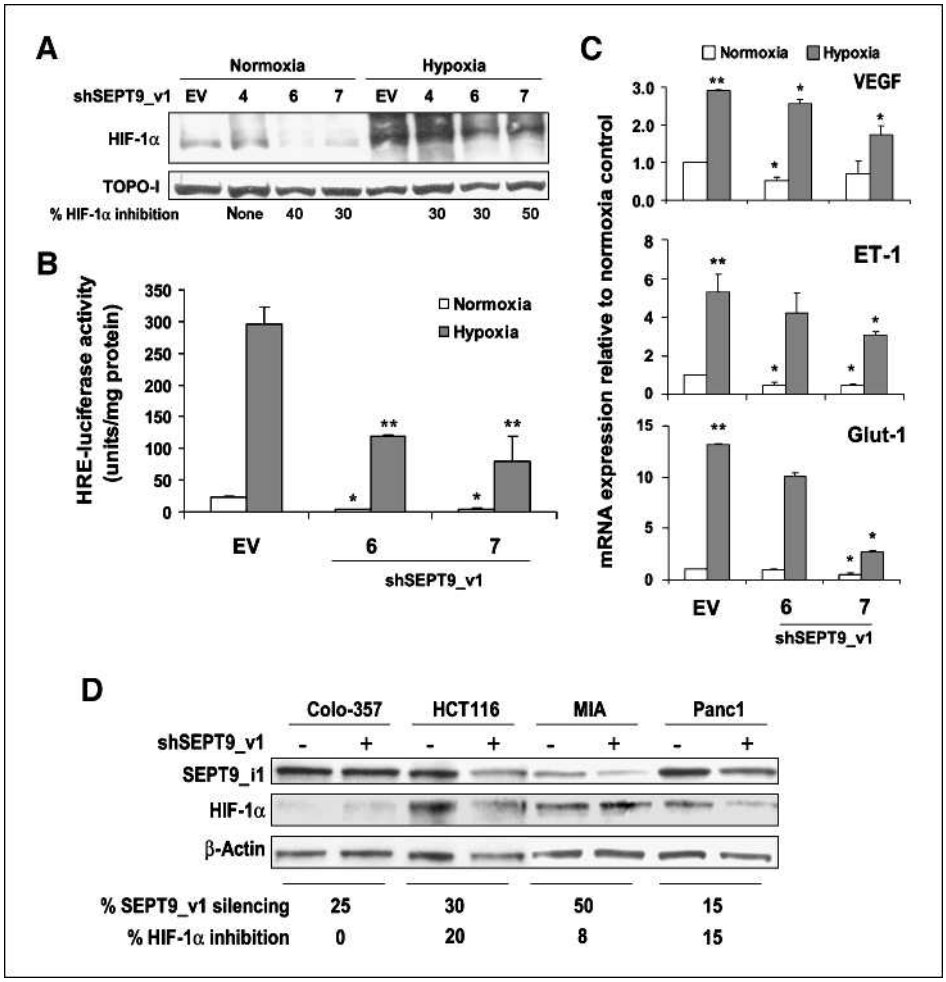

FIGURE 2. SEPT9_v1 KD downregulates HIF-1α protein expression and inhibits HIF-1 transcriptional activity. A, puromycin-resistant PC-3 cells stably expressing EV or shSEPT9_v1 (clones 4, 6, and 7) were grown under normoxia and hypoxia. Nuclear extracts were prepared, analyzed by SDS-PAGE, and immunoblotted with antibodies to HIF-1α and TOPO-I. The HIF-1α protein levels shown below the respective lanes were quantified by densitometry and normalized to TOPO-I. B, the PC-3 stably infected EV cells and shSEPT9_v1 clones 6 and 7 were all transiently transfected with pBI-GL V6L (1 μg/well) expressing luciferase under the control of HRE. After 24 h of transfection, the cells were grown overnight under normoxia and hypoxia and then analyzed for luciferase luminescence assay. Relative luciferase activity represents units per milligram of protein at each assay point. Columns, mean (n = 3); bars, SD. *, $P < 0.001$, between shSEPT9_v1 and EV control under normoxia; **, $P < 0.01$, between shSEPT9_v1 and EV control under hypoxia. C, total RNA was isolated from puromycin-resistant EV cells and shSEPT9_v1 clones 6 and 7 were grown under normoxia and hypoxia. Real-time PCR was done to amplify VEGF, Glut-1, ET-1, and β-actin mRNA. mRNA levels normalized to β-actin were drawn relative to normoxia controls for each gene. Columns, mean (n = 4); bars, SD. *, $P < 0.05$, between EV and shSEPT9_v1 (inhibition) at normoxia or hypoxia; **, $P < 0.05$, between EV normoxia and hypoxia. D, the indicated cancer cells were transiently transfected with pSUPER.retro.puro EV or expressing shSEPT9_v1 and grown under normoxic conditions. After 48 h, WCEs were prepared, analyzed by SDS-PAGE, and immunoblotted with antibodies to SEPT9_i1, HIF-1α, and actin. SEPT9_i1 and HIF-1α protein levels were quantified by densitometry and normalized to actin.

for each antibody, treated with 3% H_2O_2, and processed for immunostaining with anti-CD34, anti-Ki67, anti–caspase-3, and anti-SEPT9_i1 in CAS-Block (Zymed Laboratories) overnight at 4°C. On the next day, the slides were washed with Optimax (Biogenex), incubated for 30 minutes at room temperature with secondary antibody, and developed with 3,3′-diaminobenzidine. Sections were counterstained with hematoxylin. The microvessel density (MVD), percentage of Ki67-positive stained nuclei, and number of caspase-3–positive stained cells were quantified in ×40 magnification fields and compared between control EV and shSEPT9_v1 tumors.

Protein extraction of xenograft tumors. Tumor tissue (10 mg) was manually homogenized in 20 mmol/L Tris (pH 7.4), 4 mmol/L EDTA, and 2% SDS supplemented with protease inhibitors; incubated on ice for 30 minutes; and then cleared by centrifugations. Protein extracts were analyzed as described above.

Data analysis. The experiments presented in the figures are representative of three or more independent repetitions. Quantification of band densities was done with TINA software version 2.0. The data are expressed as mean ± SD or mean ± SEM as indicated in the figure legends. Student's t test and ANOVA were used to compare

Published OnlineFirst April 20, 2010; DOI: 10.1158/1541-7786.MCR-09-0497

differences between particular conditions. Significance was set at $P < 0.05$.

Results

SEPT9_v1 silencing downregulates the HIF-1 pathway in prostate cancer cells. We used RNAi methodology to study the effects of SEPT9_i1 downregulation on HIF-1. *SEPT9* can theoretically be transcribed up to 18 splice variants generating six mRNAs with different NH_2 termini (SEPT9_v1, SEPT9_v2, SEPT9_v3, SEPT9_v4, SEPT9_v4*, and SEPT9_v5) as well as three possible indistinguishable mRNA ends (a, b and c; ref. 24). To exclusively knock down SEPT9_v1 variant, we designed several siRNAs targeting the unique sequence that encodes the first 25 amino acids of SEPT9_i1. We identified a siRNA that specifically knocks down SEPT9_v1 and downregulates SEPT9_i1 protein expression but not other expressed isoforms in PC-3 cells (Fig. 1A). This sequence was designed as a short hairpin (shRNA) and was constructed into a viral vector (pSUPER.retro.puro) to produce stable expression in PC-3 prostate cancer cells. Puromycin-selected clones from PC-3 infected with the EV control and shRNA to GFP or to SEPT9_v1 were tested for SEPT9_i1 downregulation (Fig. 1B). Neither the EV nor the shRNA to GFP caused any noticeable SEPT9_i1 inhibition compared with parental PC-3 cells (data not shown). We therefore used pooled clones of EV as control for comparison with the shSEPT9_v1 different clones. SEPT9_v1 silencing in shSEPT9_v1 clones was confirmed using quantitative real-time reverse transcription-PCR (Fig. 1C). We observed ~50% significant inhibition of SEPT9_v1 mRNA levels compared with EV cells.

Consistent with our previous results showing that SEPT9_i1 upregulates HIF-1α (8), nuclear HIF-1α protein levels were reduced in accordance with SEPT9_i1 inhibition under both normoxia and hypoxia (Fig. 2A). We next tested the effects of SEPT9_v1 knockdown (KD) on HIF-1 transcriptional activity by using a HRE-dependent reporter gene assay (Fig. 2B) and by determining transcript levels of HIF-1 target genes (Fig. 2C). SEPT9_v1 KD significantly inhibited HIF-1 transcriptional activity by 70% to 85% under normoxia and by 60% to 75% under hypoxia (Fig. 2B). Similarly, the transcript levels of select HIF-1target genes (*VEGF, ET-1*, and *Glut-1*) analyzed by quantitative real-time reverse transcription-PCR were also inhibited in SEPT9_v1 KD PC-3 cells under normoxia and hypoxia (Fig. 2C). These results show that inhibition of SEPT9_i1 expression by RNAi causes downregulation of both HIF-1α protein expression and HIF-1 transcriptional activity.

To extend our studies on SEPT9_v1 KD in human cancer cells other than those of the prostate, we transiently expressed shSEPT9_v1 in cancer cells of the colon (Colo-357 and HCT116) and pancreas (MIA and Panc1). Inhibition of SEPT9_i1 expression was obtained in various degrees under the same conditions of transfection used in PC-3 cells (Fig. 2D). KD of SEPT9_v1 inhibited HIF-1α protein expression in HCT116 and Panc1 cells but not in Colo-357 and MIA cells (Fig. 2D). These results suggest that the dependence of HIF-1α protein expression on SEPT9_i1 is not absolute and may vary among different cancer cells.

SEPT9_v1 KD decreases HIF-1α protein expression by accelerating its ubiquitination and proteasomal degradation. SEPT9_i1 stabilizes HIF-1α protein by preventing its RACK1-dependent ubiquitination and degradation through the proteasome (13). We therefore examined whether downregulation of HIF-1 by SEPT9_i1 KD is a result of increased ubiquitination and degradation of HIF-1α protein. Control and SEPT9_v1 KD PC-3 cells were treated with increasing concentrations of the proteasome inhibitor MG-132 (Fig. 3A). Reduction in HIF-1α protein levels was almost completely reversed by proteasome inhibition (Fig. 3A). Furthermore, ubiquitination of HIF-1α protein was dramatically facilitated in SEPT9_v1 KD cells compared with EV control cells (Fig. 3B). Taken together, these experiments showed that downregulation of SEPT9_i1 suppresses HIF-1α protein expression and

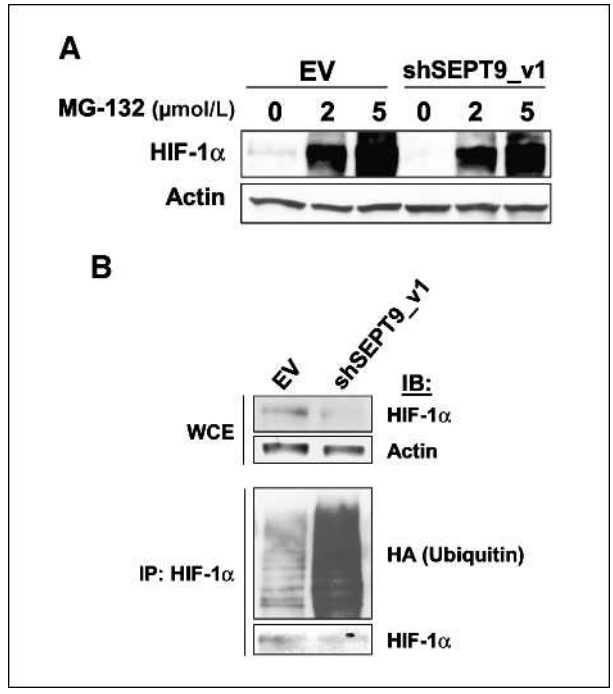

FIGURE 3. SEPT9_v1 KD accelerates HIF-1α protein ubiquitination and degradation. A, puromycin-resistant EV and shSEPT9_v1 PC-3 cells were treated with increased concentrations of MG-132 for 4 h under normoxic conditions. WCEs were prepared, analyzed by SDS-PAGE, and immunoblotted with antibodies to HIF-1α and β-actin. B, the stably infected EV and shSEPT9_v1 PC-3 cells were transiently transfected with expressing vector encoding HA-ubiquitin. After 48 h, WCEs were prepared and equal amounts of the extracted proteins were subjected to immunoprecipitation (IP) with antibodies to HIF-1α. The whole amount of eluted immunoprecipitates from each condition was loaded on SDS-PAGE and then analyzed by immunoblotting (IB) with antibodies to HIF-1α and HA. In parallel, WCEs were also analyzed by immunoblotting with antibodies to HIF-1α and β-actin.

Published OnlineFirst April 20, 2010; DOI: 10.1158/1541-7786.MCR-09-0497

HIF-1 transcriptional activity by increasing HIF-1α protein ubiquitination and degradation through the proteasome.

SEPT9_v1 KD suppresses tumorigenicity of prostate cancer cells. We had shown that SEPT9_v1 KD affects cell viability and inhibits proliferation of prostate cancer cells (18). Expanding those studies, we now investigated the effects of SEPT9_v1 KD on other cellular functions. We characterized the changes in cellular morphology after SEPT9_v1 silencing using Giemsa staining of cytospin preparations. The morphologic differences observed between EV and KD cells were mainly in cell size, nucleus shape, cytoplasm color, and membrane surface (Fig. 4A). SEPT9_v1 KD cells also had an increased nuclear-cytoplasm ratio. The nuclei of SEPT9_v1 KD cells were kidney shaped, and the membranes were smooth compared with EV cells, which had round nuclei and serrated membranes (Fig. 4A; Supplementary Fig. S1). All these morphologic changes indicate that SEPT9_v1 KD has disrupted cell integrity.

SEPT9_i1 overexpression was shown to affect the cell cycle (25, 26). Therefore, we studied the consequences of SEPT9_i1 downregulation on the cell cycle by fluorescence-activated cell sorting (FACS) analysis (Fig. 4B). Quantification of the FACS data revealed that the number of cells in the G_0-G_1 phase was significantly higher in SEPT9_v1 KD cells compared with control cells (50 ± 4% versus 40 ± 4%, respectively; $P = 0.03$), whereas the number of cells was lower in the S phase (23 ± 5.6% versus 35 ± 2.3%, respectively; $P = 0.04$; Fig. 4B, bottom). There was no significant difference between the cells in the G_2-M phase.

Another oncogenic phenotype of SEPT9_v1 is increased cell migration and motility (14, 26). Using the scrape wound-healing migration assay, we found that SEPT9_v1 KD significantly decreased migration compared with controls even after a short period of time where proliferation does not take place (Fig. 4C). This result indicates that reducing SEPT9_i1 levels decreases the invasive potential in these cells. Altogether, the results provide additional molecular evidence that SEPT9_i1 is a positive factor in tumorigenesis.

SEPT9_i1 depletion inhibits tumor growth in a prostate cancer xenograft model. We used a xenograft model to study the consequences of SEPT9_v1 KD *in vivo*. Two different PC-3 clones expressing shRNA to SEPT9_v1

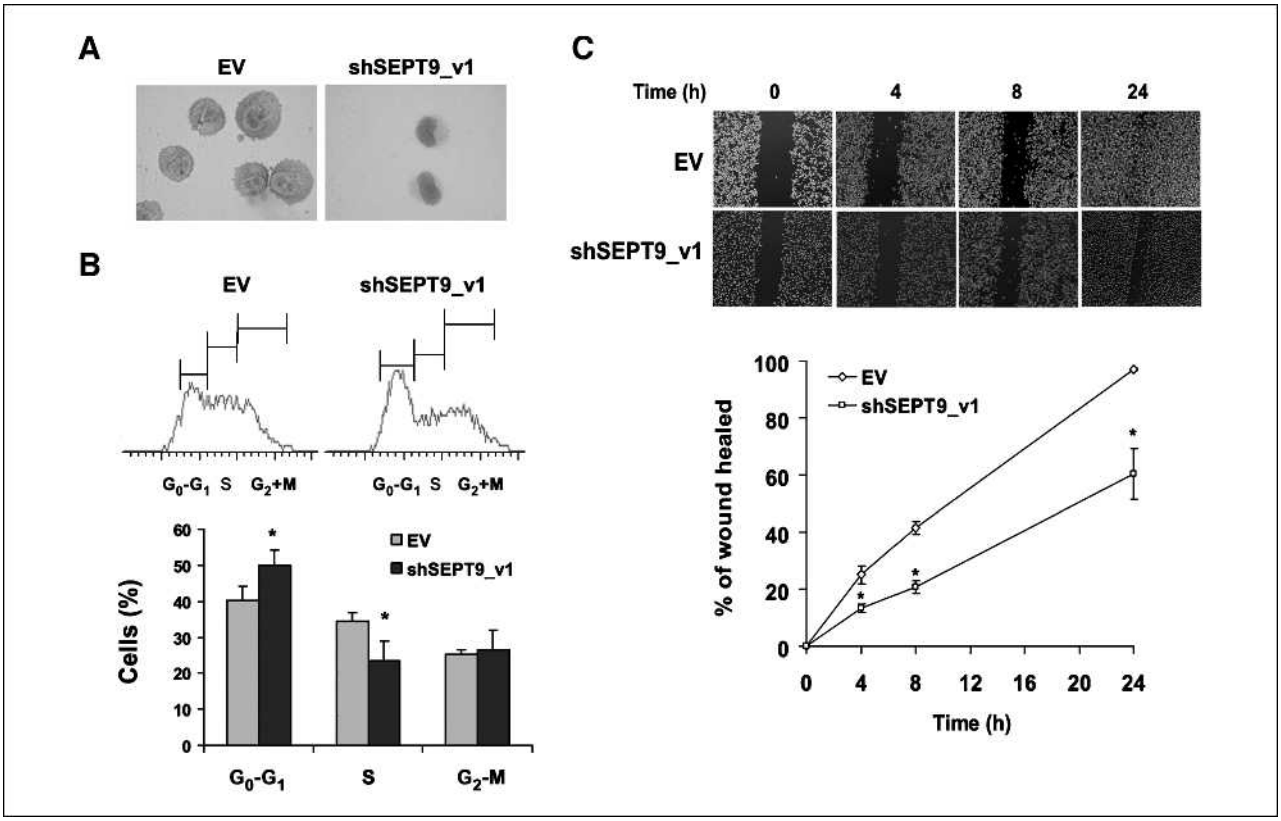

FIGURE 4. SEPT9_v1 silencing disrupts cell shape, dysregulates cell cycle, and inhibits migration. A, representative cytospin smear containing puromycin-resistant EV and shSEPT9_v1 PC-3 cells was stained using Giemsa. B, top, cell cycle histograms generated by FACS analysis of puromycin-resistant EV and shSEPT9_v1 PC-3 cells; bottom, quantification of the FACS analysis representing the percentage of cells in each phase of the cell cycle derived from three independent experiments done in duplicates. Columns, average of the means ($n = 3$); bars, SD. *, $P < 0.04$. C, stably infected EV and shSEPT9_v1 PC-3 cells were seeded in six-well plates for 70% confluent. The cell monolayer was scratched with a sterile pipette tip after 24 h. The wounded cultures were photographed after 4, 8, and 25 h (top), and the percentage of wound healing was calculated (bottom) as described in Materials and Methods. Points, mean ($n = 2$); bars, SD. *, $P < 0.04$.

Published OnlineFirst April 20, 2010; DOI: 10.1158/1541-7786.MCR-09-0497

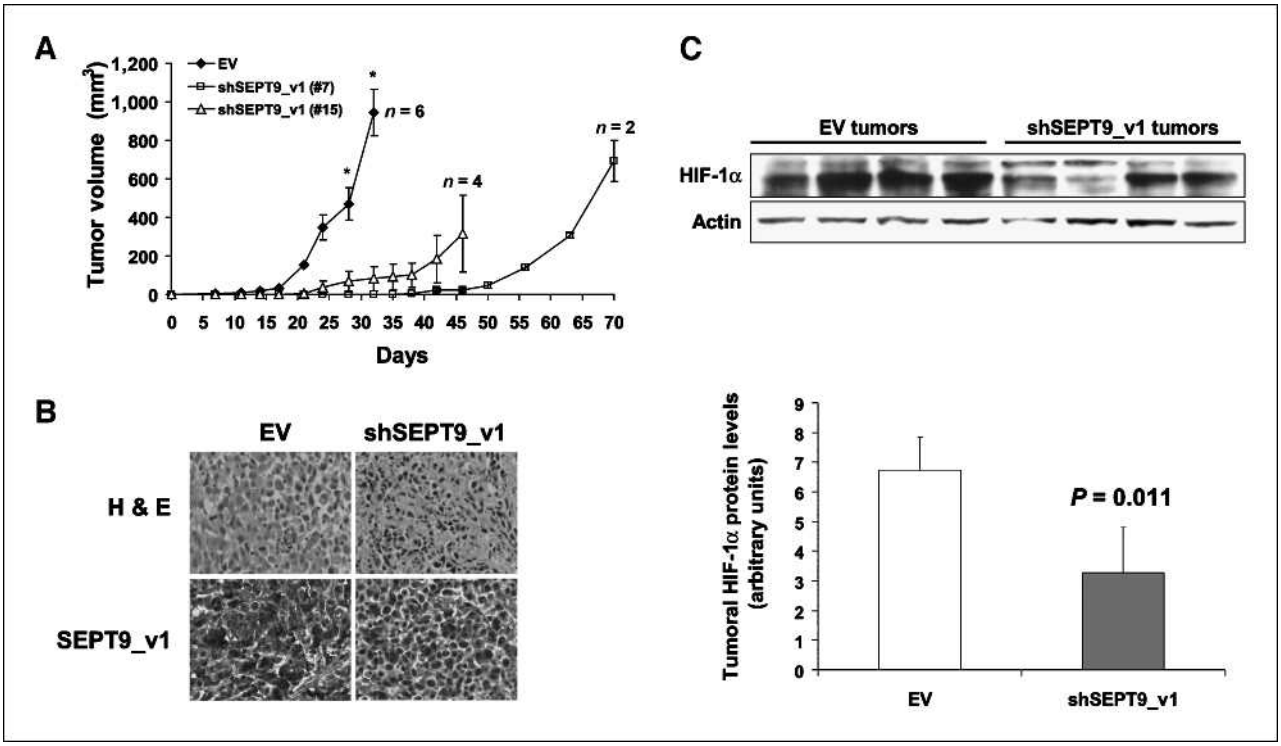

FIGURE 5. SEPT9_v1 KD inhibits tumor growth and HIF-1α protein expression *in vivo*. A, a prostate cancer xenograft model was established using stably infected EV and shSEPT9_v1 PC-3 cells (2×10^6) implanted s.c. into hinds of athymic nude mice. Tumor size was measured twice a week, and its volume was determined. Points, mean; bars, SE. *, $P < 0.05$, between EV and shSEPT9_v1 groups. B, bottom, sections from EV and shSEPT9_v1 tumors were stained with H&E or immunostained with anti-SEPT9_i1 antibodies. C, top, protein extracts were prepared from four representative xenograft tumors from each group and analyzed by Western blotting using antibodies to HIF-1α and actin; bottom, densitometric quantification of normalized HIF-1α levels to actin.

and EV control PC-3 cells were injected into athymic nude mice. The take rate of SEPT9_v1 KD cells in these mice was relatively low and ranged from 0% to 66% in comparison with the 100% take rate of the EV clones. shSEPT9_v1 clones showed significant retardation in tumor growth rate by a 2- to 3-fold longer interval time after injection than the controls and reached smaller dimensions (Fig. 5A).

After the animals were sacrificed, the tumors were excised and analyzed by immunohistochemical staining. SEPT9_i1 staining confirmed SEPT9_i1 downregulation in the majority of the cells (Fig. 5B). Western blot analysis of tumors extracts showed that the expression of HIF-1α protein levels within the shSEPT9_v1 tumors was significantly lower than in control tumors (Fig. 5C). Tumors derived from SEPT9_v1 KD cells exhibited a dramatic reduction in MVD and a significant inhibition of intratumoral cell proliferation, quantified by Ki67 staining, compared with control tumors (Fig. 6). Consistent with previous reports that SEPT9_v1 does not affect apoptosis (14), the difference in caspase-3 staining was not significant among the tumors (Fig. 6). Taken together, our *in vivo* data show that depletion of intracellular SEPT9_i1 by RNAi decreases tumorigenicity and inhibits angiogenesis concomitant with HIF-1 downregulation in this prostate cancer model.

Inhibition of cell proliferation by SEPT9_i1 silencing is mediated by HIF-1. To determine whether the effects of SEPT9_v1 silencing on tumor growth are mediated by the HIF-1 pathway, we used the genetically manipulated HIF-1α knockout colon cancer cells (HCT116$^{HIF\text{-}1\alpha-/-}$) previously designed by Dang et al. (17). These cells neither express HIF-1α protein nor exhibit transcriptional activity of HIF-1 as measured by reporter gene assay (data not shown). We measured the proliferation rate of these cells and of their parental HCT116 counterpart cells before and after SEPT9_v1 silencing (Fig. 7). As expected (17), the proliferation rate of HCT116$^{HIF\text{-}1\alpha-/-}$ cells was significantly decreased compared with parental HCT116 cells (Fig. 7A). Consistent with our previous results (18), SEPT9_v1 silencing (Fig. 7B) caused >50% significant inhibition of proliferation in parental HCT116 cells, whereas it did not affect proliferation at all in HCT116$^{HIF\text{-}1\alpha-/-}$ cells (Fig. 7A). These results highly suggest that the major antiproliferative effect of shSEPT9_v1 is mediated by the HIF-1 pathway.

Discussion

Mammalian SEPT9 isoforms have been implicated in several oncogenic pathways, including Rho signaling

Published OnlineFirst April 20, 2010; DOI: 10.1158/1541-7786.MCR-09-0497

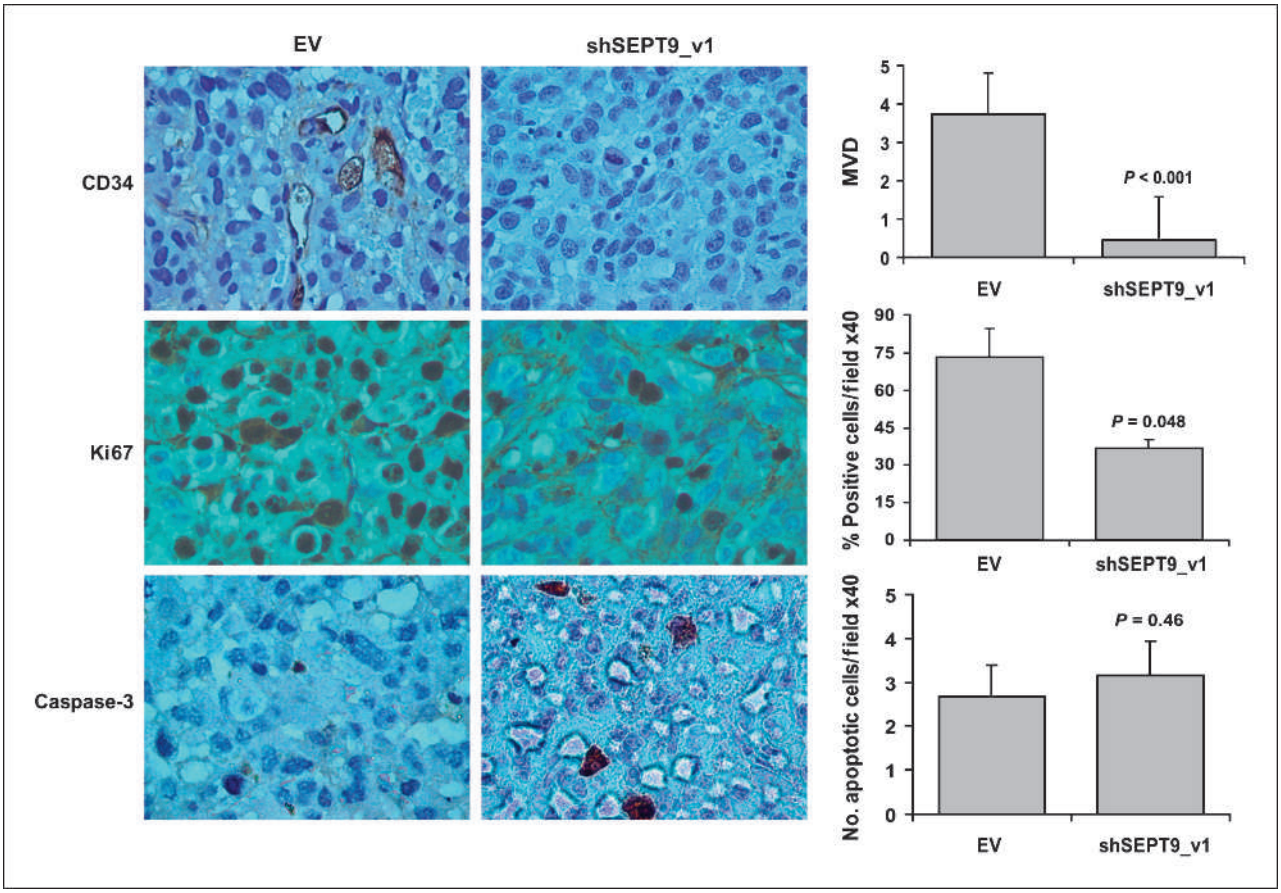

FIGURE 6. shSEPT9_v1 KD inhibits intratumor angiogenesis and cell proliferation but does not induce apoptosis. CD34 immunostaining (×20; top), Ki67 (×40; middle), and caspase-3 (×40; bottom) of representative tumor sections from different EV and shSEPT9_v1 PC-3 xenograft groups. Graphs represent total CD34-positive microvessels normalized by section areas, MVD, % of Ki67-positive cells, and number of apoptotic cells per field (×40), respectively. Columns, average (four mice per group) of the means (five sections per tumor); bars, SE.

(SEPT9_i3; ref. 27), migration (SEPT9_i4; ref. 28), hypoxia (SEPT9_i1; refs. 8, 13), and c-Jun NH_2-terminal kinase (SEPT9_i1; ref. 26). In this study, we provided evidence that SEPT9_i1 can be targeted to inhibit growth and angiogenesis of human prostate cancer cells.

We found that downregulating SEPT9_i1 by specific shRNA leads to reduction in HIF-1α protein expression with respective inhibition of HIF-1 transcriptional activity (Fig. 2). SEPT9_i1 stabilizes HIF-1α protein by preventing its RACK1-dependent ubiquitination and degradation pathway (8, 13). RACK1 competes with heat shock protein 90 (HSP90) for binding to HIF-1α and in mediating its O_2-independent ubiquitination and proteasomal degradation (29, 30). We show here that SEPT9_v1 KD enhances HIF-1α ubiquitination and degradation in prostate cancer cells (Fig. 3). The heterogeneity in HIF-1α inhibition by SEPT9_v1 KD might be influenced by a "fine balance" existing between RACK1/HSP90 and HIF-1α/SEPT9_i1 levels in a given cancer cell. Further studies are necessary to elucidate the dynamics among these cellular functions in the different cell types. It would be worthwhile to test whether combining HSP90 inhibitors with SEPT9_v1 silencing will allow more efficient total downregulation of HIF-1α in target tumors.

The effects of SEPT9_i1 depletion on cell integrity were robust. It induced marked morphologic changes and dysregulated cell cycle (Fig. 4). Puromycin-resistant PC-3 cells distinguished by dramatic inhibition (>80%) of SEPT9_i1 became senescent after a small number of passages (from two to three) and could not be maintained in culture.[1] SEPT9_v1 KD was shown to decrease proliferation in prostate (18) and breast (14) cancer cells *in vitro*. The antiproliferative effects of SEPT9_v1 silencing were abolished in the colon cancer cells that do not express HIF-1α (Fig. 7). SEPT9_v1 KD also inhibited cell proliferation *in vivo* in our prostate cancer model (Fig. 6). The antiproliferative consequences of SEPT9_i1 depletion could be attributed not only to the effects on HIF-1 but also to the effects of SEPT9_v1 KD on the c-Jun NH_2-terminal kinase/cyclin D1 pathway (26).

[1] Personal observation.

Published OnlineFirst April 20, 2010; DOI: 10.1158/1541-7786.MCR-09-0497

Quantification of the extent of migration revealed that PC-3 cells expressing shSEPT9_v1 exhibited a dramatic decrease (75%) in cell motility compared with the control cells (Fig. 4C). Furthermore, *in vivo* data showed that the reduction in MVD was more prominent than the intratumoral proliferation (Fig. 6). These results suggest that SEPT9_i1 affects invasiveness, rather than proliferation, when determining the tumorigenic-metastatic potential of these cells. Our results, which show the significance of SEPT9_i1 in the invasive process, are corroborated by those of Chacko et al. (28) who showed that SEPT9_i4 isoform expression enhances cell motility and is associated with perturbation of directional movement, leading to phenotypes associated with neoplasia.

As mentioned earlier, SEPT9_v1 KD tumors appeared after a significant delay and reached much smaller volumes compared with EV controls at the same time point (Fig. 5). These results were obtained concomitantly with the effects of SEPT9_v1 KD on the HIF-1 pathway *in vivo*. HIF-1α protein expression levels in SEPT9_v1 KD tumors were significantly lower than in the EV tumors (Fig. 5C), with a respective decrease in angiogenesis (Fig. 6). HIF-1α levels and MVD were analyzed at the time of sacrifice when the tumors were growing exponentially: they still exhibited significant reductions in HIF-1α and blood vessel levels. These results indicate that the effects of SEPT9_v1 KD on tumor establishment, growth, and angiogenesis are mediated, at least in a significant part, by the HIF-1 pathway. Attainment of tumor cells to create new blood vessels is an important aspect of tumor progression. Disruption of the HIF-1 pathway by SEPT9_v1 KD apparently significantly delayed the turning on of the "angiogenic switch."

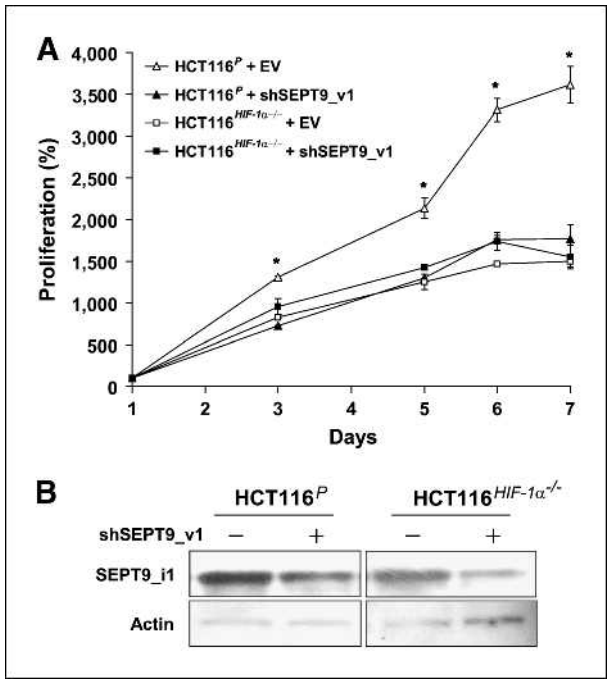

FIGURE 7. SEPT9_v1 KD inhibits cell proliferation in a HIF-1–dependent fashion. Parental HCT116 ($HCT116^{P}$) and $HCT116^{HIF\text{-}1\alpha-/-}$ cells were transiently transfected with EV or shSEPT9_v1. A, after 24 h of transfection (day "0"), cells were seeded in 96-well plates and processed for XTT proliferation assay at the indicated times. Proliferation was expressed as increase in percentage of the initial absorbance that was measured 24 h after seeding (100% at day "1"). Points, mean ($n = 3$); bars, SD. *, $P < 0.001$, between $HCT116^{P}$ + EV and $HCT116^{P}$ + shSEPT9_v1, and between $HCT116^{P}$ + EV and $HCT116^{HIF\text{-}1\alpha-/-}$ + EV. B, after 48 h of transfection, WCEs were prepared and analyzed for SEPT9_i1 silencing by SDS-PAGE and immunoblotting with antibodies to SEPT9_i1 and β-actin.

In summary, the results of the current study show that using RNAi to reduce SEPT9_i1 levels in prostate cancer cells significantly reduces the expression of HIF-1α protein, cellular proliferation, motility, angiogenesis, and tumor growth *in vivo*. Further investigations are required to test which routes of delivery (e.g., direct intratumoral injections or systemic administration) of shSEPT9_v1 would be most efficient for prostate cancer therapy.

Disclosure of Potential Conflicts of Interest

No potential conflicts of interest were disclosed.

Acknowledgments

We thank Dr. Ben-Zion Katz (Department of Hematology, Tel Aviv Sourasky Medical Center, Tel Aviv, Israel) for help with the morphologic and FACS analyses, Dr. Pikarsky and his group (Department of Pathology, Hadassah-Hebrew University Medical Center, Jerusalem, Israel) for their assistance with immunohistochemical staining, and Esther Eshkol for editorial assistance.

Grant Support

Prostate Cancer Foundation, M.K. Humanitarian Foundation, and Dr. Miriam and Sheldon G. Adelson Medical Research Foundation.

The costs of publication of this article were defrayed in part by the payment of page charges. This article must therefore be hereby marked *advertisement* in accordance with 18 U.S.C. Section 1734 solely to indicate this fact.

Received 11/09/2009; revised 02/28/2010; accepted 03/25/2010; published OnlineFirst 04/20/2010.

Published OnlineFirst April 20, 2010; DOI: 10.1158/1541-7786.MCR-09-0497

References

1. Semenza GL. Hypoxia and cancer. Cancer Metastasis Rev 2007;26:223–4.
2. Brown JM, Wilson WR. Exploiting tumour hypoxia in cancer treatment. Nat Rev Cancer 2004;4:437–47.
3. Hockel M, Vaupel P. Tumor hypoxia: definitions and current clinical, biologic, and molecular aspects. J Natl Cancer Inst 2001;93:266–76.
4. Semenza GL. Regulation of oxygen homeostasis by hypoxia-inducible factor 1. Physiology (Bethesda) 2009;24:97–106.
5. Melillo G. Targeting hypoxia cell signaling for cancer therapy. Cancer Metastasis Rev 2007;26:341–52.
6. Melillo G. Inhibiting hypoxia-inducible factor 1 for cancer therapy. Mol Cancer Res 2006;4:601–5.
7. Rapisarda A, Hollingshead M, Uranchimeg B, et al. Increased antitumor activity of bevacizumab in combination with hypoxia inducible factor-1 inhibition. Mol Cancer Ther 2009;8:1867–77.
8. Amir S, Wang R, Matzkin H, Simons JW, Mabjeesh NJ. MSF-A interacts with hypoxia-inducible factor-1α and augments hypoxia-inducible factor transcriptional activation to affect tumorigenicity and angiogenesis. Cancer Res 2006;66:856–66.
9. Barral Y, Kinoshita M. Structural insights shed light onto septin assemblies and function. Curr Opin Cell Biol 2008;20:12–8.
10. Weirich CS, Erzberger JP, Barral Y. The septin family of GTPases: architecture and dynamics. Nat Rev Mol Cell Biol 2008;9:478–89.
11. Russell SE, Hall PA. Do septins have a role in cancer? Br J Cancer 2005;93:499–503.
12. Garcia W, de Araujo AP, Neto Mde O, et al. Dissection of a human septin: definition and characterization of distinct domains within human SEPT4. Biochemistry 2006;45:13918–31.
13. Amir S, Wang R, Simons JW, Mabjeesh NJ. SEPT9_v1 up-regulates hypoxia-inducible factor 1 by preventing its RACK1-mediated degradation. J Biol Chem 2009;284:11142–51.
14. Gonzalez ME, Peterson EA, Privette LM, Loffreda-Wren JL, Kalikin LM, Petty EM. High SEPT9_v1 expression in human breast cancer cells is associated with oncogenic phenotypes. Cancer Res 2007;67:8554–64.
15. Demichelis F, Fall K, Perner S, et al. TMPRSS2: ERG gene fusion associated with lethal prostate cancer in a watchful waiting cohort. Oncogene 2007;26:4596–9.
16. Setlur SR, Mertz KD, Hoshida Y, et al. Estrogen-dependent signaling in a molecularly distinct subclass of aggressive prostate cancer. J Natl Cancer Inst 2008;100:815–25.
17. Dang DT, Chen F, Gardner LB, et al. Hypoxia-inducible factor-1α promotes nonhypoxia-mediated proliferation in colon cancer cells and xenografts. Cancer Res 2006;66:1684–936.
18. Amir S, Mabjeesh NJ. SEPT9_V1 protein expression is associated with human cancer cell resistance to microtubule-disrupting agents. Cancer Biol Ther 2007;6:1926–31.
19. Mabjeesh NJ, Escuin D, LaVallee TM, et al. 2ME2 inhibits tumor growth and angiogenesis by disrupting microtubules and dysregulating HIF. Cancer Cell 2003;3:363–75.
20. Post DE, Van Meir EG. Generation of bidirectional hypoxia/HIF-responsive expression vectors to target gene expression to hypoxic cells. Gene Ther 2001;8:1801–7.
21. Mabjeesh NJ, Post DE, Willard MT, et al. Geldanamycin induces degradation of hypoxia-inducible factor 1α protein via the proteosome pathway in prostate cancer cells. Cancer Res 2002;62:2478–82.
22. Wesley UV, Bove PF, Hristova M, McCarthy S, van der Vliet A. Airway epithelial cell migration and wound repair by ATP-mediated activation of dual oxidase 1. J Biol Chem 2007;282:3213–20.
23. Pikarsky E, Porat RM, Stein I, et al. NF-κB functions as a tumour promoter in inflammation-associated cancer. Nature 2004;431:461–6.
24. Scott M, McCluggage WG, Hillan KJ, Hall PA, Russell SE. Altered patterns of transcription of the septin gene, SEPT9, in ovarian tumorigenesis. Int J Cancer 2006;118:1325–9.
25. Surka MC, Tsang CW, Trimble WS. The mammalian septin MSF localizes with microtubules and is required for completion of cytokinesis. Mol Biol Cell 2002;13:3532–45.
26. Gonzalez ME, Makarova O, Peterson EA, Privette LM, Petty EM. Up-regulation of SEPT9_v1 stabilizes c-Jun-N-terminal kinase and contributes to its pro-proliferative activity in mammary epithelial cells. Cell Signal 2009;21:477–87.
27. Nagata K, Inagaki M. Cytoskeletal modification of Rho guanine nucleotide exchange factor activity: identification of a Rho guanine nucleotide exchange factor as a binding partner for Sept9b, a mammalian septin. Oncogene 2005;24:65–76.
28. Chacko AD, Hyland PL, McDade SS, Hamilton PW, Russell SH, Hall PA. SEPT9_v4 expression induces morphological change, increased motility and disturbed polarity. J Pathol 2005;206:458–65.
29. Liu YV, Baek JH, Zhang H, Diez R, Cole RN, Semenza GL. RACK1 competes with HSP90 for binding to HIF-1α and is required for O(2)-independent and HSP90 inhibitor-induced degradation of HIF-1α. Mol Cell 2007;25:207–17.
30. Liu YV, Semenza GL. RACK1 vs. HSP90: competition for HIF-1 α degradation vs. stabilization. Cell Cycle 2007;6:656–9.
31. Gewirtz AM. On future's doorstep: RNA interference and the pharmacopeia of tomorrow. J Clin Invest 2007;117:3612–4.
32. Grimm D. Small silencing RNAs: state-of-the-art. Adv Drug Deliv Rev 2009;61:672–703.
33. Li L, Lin X, Staver M, et al. Evaluating hypoxia-inducible factor-1α as a cancer therapeutic target via inducible RNA interference *in vivo*. Cancer Res 2005;65:7249–58.
34. Gillespie DL, Whang K, Ragel BT, Flynn JR, Kelly DA, Jensen RL. Silencing of hypoxia inducible factor-1α by RNA interference attenuates human glioma cell growth *in vivo*. Clin Cancer Res 2007;13:2441–8.

Published OnlineFirst April 20, 2010; DOI: 10.1158/1541-7786.MCR-09-0497

Molecular Cancer Research

Targeted Knockdown of SEPT9_v1 Inhibits Tumor Growth and Angiogenesis of Human Prostate Cancer Cells Concomitant with Disruption of Hypoxia-Inducible Factor-1 Pathway

Sharon Amir, Maya Golan and Nicola J. Mabjeesh

Mol Cancer Res 2010;8:643-652. Published OnlineFirst April 20, 2010.